Aggregation and Electrolyte Composition Effects on the Efficiency of Dye-Sensitized Solar Cells. A Case of a Near-Infrared Absorbing Dye for Tandem Cells

ARTICLE *in* THE JOURNAL OF PHYSICAL CHEMISTRY C · JANUARY 2014

Impact Factor: 4.77 · DOI: 10.1021/jp410106k

6 AUTHORS, INCLUDING:

Marcin Ziolek
Adam Mickiewicz University
53 PUBLICATIONS **823** CITATIONS
SEE PROFILE

Yan Hao
Uppsala University
27 PUBLICATIONS **468** CITATIONS
SEE PROFILE

Haining Tian
Uppsala University
46 PUBLICATIONS **2,347** CITATIONS
SEE PROFILE

THE JOURNAL OF PHYSICAL CHEMISTRY C

Article

pubs.acs.org/JPCC

Aggregation and Electrolyte Composition Effects on the Efficiency of Dye-Sensitized Solar Cells. A Case of a Near-Infrared Absorbing Dye for Tandem Cells

Marcin Ziółek,*[,†] Jerzy Karolczak,[†,‡] Maciej Zalas,[§] Yan Hao,[∥] Haining Tian,[⊥] and Abderrazzak Douhal*[,#]

[†]Quantum Electronics Laboratory, Faculty of Physics, Adam Mickiewicz University, Umultowska 85, 61-614 Poznan, Poland

[‡]Center for Ultrafast Laser Spectroscopy, Adam Mickiewicz University, Umultowska 85, 61-614 Poznan, Poland

[§]Faculty of Chemistry, Adam Mickiewicz University, Umultowska 89b, 61-614 Poznan, Poland

[∥]State Key Laboratory of Fine Chemicals, DUT-KTH Joint Education and Research Center on Molecular Devices, Dalian University of Technology (DUT), Dalian 116024, P. R. China

[⊥]School of Chemical Science and Engineering, Department of Chemistry, KTH Royal Institute of Technology, 10044 Stockholm, Sweden

[#]Departamento de Química Física, Facultad de Ciencias Ambientales y Bioquímica, and Inamol, Universidad de Castilla-La Mancha, Avda. Carlos III, S.N., 45071 Toledo, Spain

Supporting Information

ABSTRACT: Time-resolved laser spectroscopy studies of complete solar cells sensitized with a near-infrared absorbing dye (HY103) and filled with different electrolytes are applied to explain their macroscopic parameters (efficiency and short-circuit current). Particular attention is paid to the effect of coadsorbent, size of cations in electrolyte (lithium vs guanidine ones), and addition of *tert*-butylpyridine. A complete deactivation scheme in the cell is revealed, and the rates of electron injection and all other processes are explored. For the most efficient electrolyte, the electron injection rate constants are 0.21 ps^{-1} from monomers and 0.07 ps^{-1} from H-aggregates. Moreover, two important and novel findings are revealed: energy transfer from the excited state of monomers to H-aggregates (with rate constants from 0.04 to 0.25 ps^{-1}) and the decrease of internal conversion rate in HY103 attached to the nanoparticles (0.01 ps^{-1}) with respect to that of free dye in solution (0.06 ps^{-1}). Thus, our study gives more clues to better understand the photobehavior of dye-sensitized solar cells.

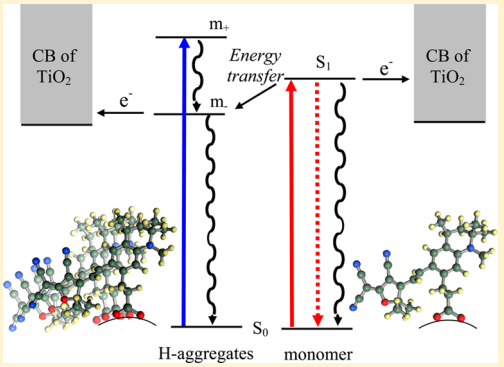

1. INTRODUCTION

Dye-sensitized solar cells (DSSCs) belong to one of the most promising emerging photovoltaic technologies.[1−3] The best solar to electricity power conversion efficiencies of DSSCs are about 12%.[4,5] To increase their performance, a new way of decreasing the photovoltage losses in DSSC devices is required.[6] Such losses occur mainly due to large driving forces that are necessary to obtain high quantum yields of partial charge separation processes: electron injection from the excited dye to the conduction band of TiO_2 nanoparticles and dye regeneration by redox couple in electrolyte (usually I_3^-/I^-). These processes occur in the fast and ultrafast time regime (from femto- to microseconds), and time-resolved laser spectroscopy techniques have to be applied for their investigation.[7] Moreover, recent results have showed that the rates of these charge separation processes are quite different in complete, operating DSSCs than in isolated systems studied before.[8−13] Therefore, new time-resolved laser spectroscopy studies of complete solar cells are important to have a good knowledge about the real rates of the charge separation processes, and the number of such studies is still lacking.

One of the ways to improve the efficiency of the solar cells is the use of tandem cells, proved by the success of multijunction semiconductor solar cells.[14] Such tandem concepts have been also tried for DSSCs, and one of the most efficient devices among them is that based on TH305 and HY103 (Figure 1A) dyes, giving the total sunlight conversion efficiency of 11.5%.[15] The redox potential of the excited state of TH305 is sufficiently negative (−1.28 V vs NHE[16]), so it is possible to energetically shift the TiO_2 conduction band edge to increase the open-circuit voltage of the solar cell. Recently, we have studied the complete solar cells sensitized with this dye by time-resolved laser spectroscopy techniques.[17] We have found a nice correlation of electron injection rate and open-circuit voltage of the device, and we confirmed that electron injection

Received: October 11, 2013
Revised: December 10, 2013
Published: December 10, 2013

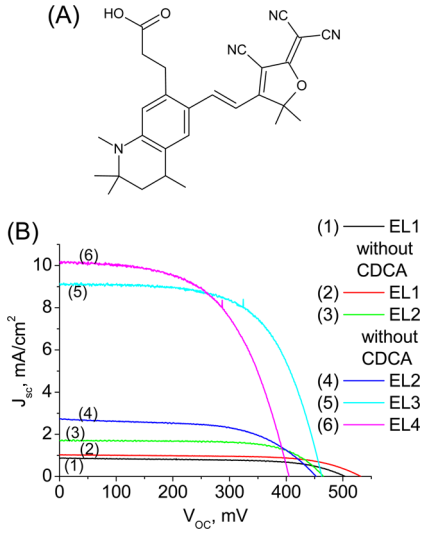

Figure 1. (A) Molecular structure of HY103. (B) Current−voltage curves for different opaque solar cells.

quantum yield can maintain a value close to 100% when the conduction band edge is shifted by electrolyte composition.

In this contribution, we focus our attention on the second dye of the tandem device—HY103. On the contrary to TH305, it was found that for good enough efficiency of HY103-sensitized solar cells a special electrolyte composition with proper amount of lithium iodide and without pyridine derivatives had to be used to move the conduction band edge of TiO_2 toward more positive potential.[15,18] This is because the redox potential of the excited state of HY103 is estimated to be much more positive (−0.87 V vs NHE[18]) than those of TH305 and other common dyes for DSSCs. The HY103 dye is also interesting from another point of view as the novel structure in which the anchoring group is separated from the acceptor groups of the dye (Figure 1A), allowing us to tune the HOMO−LUMO level in an easier way by modifying the structure of the acceptor units.[18]

Here we study complete DSSCs made of HY103 with the use of conventional current−voltage studies, stationary absorption and emission measurements, and modern time-resolved laser spectroscopy techniques. We compare the effect of adding lithium iodide, 4-*tert*-butylpyridine, and guanidine thiocyanate into iodide-based liquid electrolytes. The first two additives are the most commonly used in DSSC electrolytes,[2] while guanidine thiocyanate was found to reduce dark current of the solar cells facilitating the self-assembly of a compact dye monolayer on nanoparticles.[19,20] We also study the dye aggregation effect. The macroscopic parameters of the studied solar cells are correlated with the measured rates of the charge separation and competing processes. Very interesting results are revealed, important for a better understanding of DSSC operation and its optimization.

2. EXPERIMENTAL SECTION

HY103 dye (Figure 1A) was synthesized as previously described.[18] Acetonitrile (ACN, spectroscopic grade >99.5%, Aldrich) and dichloromethane (DCM, spectroscopic grade >99.5%, Aldrich) were used as received. Chenodeoxycholic acid (CDCA, Sigma-Aldrich) was used as coadsorbent.

Two kinds of solar cells were prepared: opaque and transparent ones, both made using slightly different methods. For the opaque cells, the procedure used for preparation of the titania electrodes was similar to those described elsewhere[21] and was as follows: 3 mL of titanium tetraisopropoxide (Aldrich) was added to 13.5 mL of ethylene glycol (Chempur) magnetically stirred at 60 °C. The mixture, after addition of 12.6 g of citric acid monohydrate (POCh), was heated under stirring at 90 °C, until clear. The obtained transparent solution was mixed with 5.6 g of P25 TiO_2 (Degussa) by grinding in agate mortar for 1 h. The viscous titania paste obtained was spread on fluorine-doped tin oxide (FTO) conductive glass substrate (Solaronix) using a "doctor blading" technique and sintered in air at 450 °C for 1 h. To prepare working electrodes for DSSCs, titania electrodes were immersed in 3×10^{-5} M solution of HY103 dye with or without CDCA (5×10^{-5} M) in DCM at 5 °C in the dark overnight. After dye adsorption, the electrodes were washed with DCM and dried in a hot air stream. Platinum film coated FTO was used as a counter electrode. The typical cell was assembled using a 25 μm thick, hot-melted, ionomeric foil (Solaronix) as a sealant and a spacer between the electrodes, and the electrolyte was injected within two holes predrilled in the counter electrode. The final sealing was realized with the use of hot melted sealant and a microscope cover slide. The typical active area of the obtained DSSC was approximately 0.125 cm^2. For each configuration three cells were prepared, and the shown results are for the best one.

For the transparent cells, Ti-Nanoxide HT paste (Solaronix SA) was employed to make the TiO_2 electrodes. For the reference electrodes, the alumina paste was obtained by mixing 1 g of Al_2O_3 nanoparticles (d < 50 nm, Sigma-Aldrich) dispersed in a solution containing: 100 mL of ethanol, 1 mL of distilled water, and 1 mL of acetic acid. With the aim to obtain a homogeneous solution, the suspension was kept at ultrasonic bath during 24 h. Then, 1.6 g of ethyl cellulose and 10 mL of α-terpineol were added into the solution (under stirring conditions and temperature of 60 °C). To get the desired viscosity, the excess of ethanol was removed with a rotary evaporator. A conductive glass sheet (FTO) of 2.5 cm × 2.5 cm was first cleaned in a detergent with water, then with distilled water, and finally with ethanol using an ultrasonic bath. A layer of paste was coated on the FTO electrode using the doctor blade technique between two parallel adhesive Scotch tapes. Finally, the film on the glass was gradually heated to 450 °C and kept at that temperature for 1 h to fabricate the TiO_2 layer. Then, the conductive glass with the titania or alumina film was immersed in a 3×10^{-5} M solution of HY103 dye with or without CDCA (5×10^{-5} M) in DCM (the same as for opaque cells) and kept at room temperature for 1 h to ensure optimum sensitizer uptake (absorbance of around 1.0 in the maximum of the HY103 visible absorption band for titania sample). The platinized counter electrode was obtained by spreading a Pt-based solution (Platisol T, Solaronix) on FTO glass by heating at 450 °C. To make a complete solar cell, the counter electrode was assembled with thermal adhesive film (25 μm Surlyn, Meltronix, Solaronix) that acts as a separator and sealing element. The different electrolytes (as well as bulk ACN for the reference samples) were introduced in the complete cells with a vacuum backfilling through a hole drilled in the counter electrodes, which was later sealed by a piece of Surlyn and a microscope coverslip. The typical active area of the obtained DSSC was approximately 1.5 cm^2.

Five different electrolytes were used. The commercial iodide-based redox electrolyte was the one from Solaronix (Iodolyte

dx.doi.org/10.1021/jp410106k | J. Phys. Chem. C 2014, 118, 194−205

AN-50), and it contains the I^-/I_3^- redox couple ($[I_2]$ = 50 mM), ionic liquid, lithium salt, and pyridine derivative in ACN solution. The other four electrolytes (EL1−EL4) were homemade and were the following: EL1, 0.6 M 1-propyl-3-methyl-imidazolium iodide (Sigma-Aldrich), 0.03 M iodine (POCh), 0.1 M guanidine thiocyanate (Fluka), and 0.5 M 4-*tert*-butylpiridine (TBP, Sigma-Aldrich) in acetonitrile (Merck); EL2, the same as EL1 but without TBP; EL3, 0.6 M 1-propyl-3-methyl-imidazolium iodide (Sigma-Aldrich), 0.06 M lithium iodide (Sigma-Aldrich), 0.1 M tetrabutylammonium iodide (Sigma-Aldrich), and 0.02 M iodine in acetonitile:valeronitrile 85:15; EL4: the same as EL3 but with higher concentration of lithium iodide (0.5 M).

For the broadband femtosecond−picosecond transient absorption measurements, the Ti:Sapphire laser system[22] and noncollinear optical parametric amplifier (NOPA) were used. The pump pulses were at 580 or 645 nm, and the IRF (pump−probe cross correlation function) was 150−200 fs (fwhm). The pump pulse energy was 270 nJ, corresponding to energy density of about 1 mJ/cm^2. The probe beam was the white light continuum generated in a 1 cm cell of water. The transient absorption measurements were performed in the spectral range of 420−720 nm and the time range of 0−500 ps. The samples (solar cells) were not moving; however, no degradation was observed during experiment, and the time constant values were averaged from three experiments made in different parts of the cells. The data were analyzed using a global fit program that performs a convolution of IRF with multiexponential function and gives wavelength-dependent amplitudes of the fitted time components.[23] The chirp of the white light continuum was about 800 fs in the given spectral range, but all the analyzed spectra were corrected for this chirp. Therefore, after correction the time origin was the same for all wavelengths used in the global analysis. The quality of the global fit was checked by examining the fits at different wavelengths and by the chi-squared values for different numbers of exponential functions.

The nanosecond flash photolysis setup was the same as previously described.[17] A pump pulse of 5 ns time duration at 640 nm and energy density of 0.3 mJ/cm^2 were used for the sample excitation. Because of the highly dispersive nature of the observed processes, the complete kinetics were obtained by combining the decays measured at several different time scales. The time-resolved spectra were constructed from fitted kinetic traces recorded in the spectral ranges 430−700 nm every 10 or 20 nm.

Femtosecond (fs) emission transients were collected using a fluorescence upconversion technique. The system described before[17] consists of a femtosecond optical parametric oscillator (Inspire Auto 100) pumped by a Ti:sapphire oscillator Mai Tai HP (Spectra Physics) and coupled to an upconversion setup. The pumping beam was adjusted at different wavelengths in the range 580−665 nm, and its polarization was set to a magic angle in respect to the fundamental beam. The typical energy of the pump pulse was 150 pJ (average beam power 18 mW), corresponding to energy density in pulse of 500 nJ/cm^2, but control experiments with 3 and 12 times smaller energy were also done. The sample was placed in a holder connected to a pair of translation stages (MTS series, Thorlabs). They move the sample in the x−y plane perpendicular to the pump beam preventing it from photodegradation during the measurements. The IRF of the apparatus was 300−350 fs (fwhm). All the upconversion measurements were performed in a 200 ps time window.

To analyze the decays in upconversion and flash photolysis experiments, extending over a large time scale, a stretched exponential function (eq 1) was used to fit the experimental transients. In the case of upconversion studies the function was convoluted with the IRF. A stretched exponential function is given by the following formula

$$A(t) = A_0 e^{-(t/\tau)^{\beta}} \tag{1}$$

This function contains two parameters: the characteristic time τ and the dispersion parameter β ($0 < \beta < 1$, lower β values mean more stretched decay, extending the decay time scale). The averaged rate constant k of the process described by function 1 can be calculated as[8]

$$k = \left(\frac{\tau}{\beta}\Gamma\left(\frac{1}{\beta}\right)\right)^{-1} \tag{2}$$

The steady-state fluorescence and UV−visible absorption spectra were measured using FluoroMax-4 (Jobin-Yvone) and JASCO V-670 or JASCO V-550, respectively. The photovoltaic characteristics of the cells were measured using a Sun 2000 class A Solar Simulator (Abet Technologies, Milford, CT, USA) equipped with an AM 1.5 G filter, with the light intensity adjusted at 100 mW/cm^{-2} using a silicon reference cell (ReRa Systems, Wijchen, The Netherlands). Current−voltage curves were recorded on a Keithley 2400 SourceMeter (Keithley, Cleveland, OH, USA). All experiments were done at 293 K.

The electron injection rate constant k_{ei} was calculated (from upconversion and femtosecond transient absorption experiments) as the difference of the averaged constants obtained for TiO_2 (k_{Ti}) and Al_2O_3 (reference, k_{Al}) cells

$$k_{ei} = k_{Ti} - k_{Al} \tag{3}$$

and the electron injection quantum yield was calculated as the ratio

$$\phi_{ei} = k_{ei}/k_{Ti} \tag{4}$$

Similarly, the dye regeneration rate constant k_{reg} was calculated (from flash photolysis experiment) as the difference of the averaged constants obtained for TiO_2 cells filled with electrolytes ($k_{electrol}$) and ACN (reference giving recombination rate, $k_{ACN} = k_{recom}$)

$$k_{reg} = k_{electrol} - k_{recom} \tag{5}$$

and the regeneration quantum yield was calculated as the ratio

$$\varphi_{reg} = \frac{k_{reg}}{k_{reg} + k_{recom}} \tag{6}$$

3. RESULTS AND DISCUSSION

3.1. Opaque Cell for Better Efficiencies. First, the solar cells with opaque titania nanoparticle layer optimized for high efficiencies were prepared, sensitized with HY103 or HY103 with CDCA, and filled with four different electrolytes: EL1, EL2, EL3, and EL4. Figure 1B shows the current−voltage characteristics of the cells studied, while Table 1A collects the parameters of the cells: short circuit current density (J_{SC}), open circuit voltage (V_{OC}), fill factor (FF), and global efficiency (η). As stated in the Introduction, for HY103 dye the conduction band edge of TiO_2 has to be shifted toward more positive values to obtain reasonable photocurrents, which decreases

dx.doi.org/10.1021/jp410106k | J. Phys. Chem. C 2014, 118, 194−205

Table 1. Values of Some Photovoltaic Parameters of the Studied Solar Cells: Short Circuit Current Density (J_{SC}), Open Circuit Voltage (V_{OC}), Fill Factor (FF), and Global Efficiency (η)[a]

(A)

cell	J_{SC} [mA/cm^2]	V_{OC} [mV]	FF [%]	η [%]
HY103/EL1	0.87	504	63	0.28
HY103+CDAC/EL1	1.03	532	65	0.36
HY103/EL2	1.75	466	67	0.55
HY103+CDCA/EL2	2.74	454	57	0.71
HY103+CDCA/EL3	9.18	463	64	2.73
HY103+CDCA/EL4	10.20	405	58	2.40

(B)

cell	J_{SC} [mA/cm^2]	V_{OC} [mV]
HY103+CDCA/Al_2O_3/AN-50	<0.1	160
HY103+CDCA/TiO_2/EL1	0.1	50
HY103/TiO_2/EL2	0.5	350
HY103+CDCA/TiO_2/EL2	0.5	390
HY103/TiO_2/AN-50	0.5	330
HY103+CDCA/TiO_2/AN-50	0.5	470
HY103+CDCA/TiO_2/EL3	2.5	440

[a]Part (A) presents the results obtained for opaque cells (all on TiO_2) while part (B) those for transparent cells.

V_{OC}. As can be seen from Table 1A, the highest efficiency (η = 2.7% with J_{SC} = 9.2 mA/cm^2) is obtained for EL3, which contains 0.06 M LiI (without TBP). It is a little bit lower than the best efficiency reported so far for this dye (3.7% with J_{SC} = 11.8 mA/cm^2).[18] When the concentration of lithium cations is increased to 0.5 M (in EL4) the photocurrent increases (up to 10.2 mA/cm^2), but the V_{OC} drops from 463 to 405 mV, resulting in the overall lower efficiency of the cell with EL4 than EL3 (Table 1A).

A drastic decrease in the photocurrent (below 3 mA/cm^2) is observed when the electrolyte with 0.1 M guanidine cations is used (EL2) instead of Li^+ (Table 1A). This suggests that larger guanidine cations do not produce the same positive shift of the conduction band as a similar amount of much smaller lithium cations (that can penetrate over some distance into the TiO_2 structure). This effect has already been observed for single atom cations of different size.[2,17,24] Moreover, adding 0.5 M TBP, a typical procedure for improving voltage for DSSCs with dyes of low LUMO potential and high driving force for electron injection,[25] results in even worse performance of HY103 solar cell (EL1). This is because the conduction band is shifted toward more negative values, which is also reflected in higher V_{OC} of EL1 (530 mV) with respect to that of EL2 (460 mV). However, unlike our previous studies of electrolyte effect for TH305 dye,[17] the differences in values of V_{OC} cannot be directly related to the shift of conduction band edge because for large differences in photocurrents the relative position of Fermi levels in TiO_2 is different. Finally, the effect of adding a coadsorbent (CDCA) to HY103 clearly improves the global efficiency of the solar cell, which was confirmed for the cells with EL1 and EL2 (Table 1A).

This is a starting point for the spectroscopic studies presented in the next sections, aiming at detailed investigation of partial charge separation processes and explanation of the observed differences in solar cell performance. For these studies we have chosen the electrolyte giving best efficiency (EL3), the one with significantly lower J_{SC} (EL2), and we also add a commercial AN-50 electrolyte for comparison.

3.2. Steady-State Absorption/Emission and Flash Photolysis Studies. More transparent cells were prepared to investigate the coadsorbent and electrolyte composition effects by time-resolved laser spectroscopy techniques. In these cells the smaller nanoparticles (diameter ~10 nm) were used; the maximum absorbance of the dyes on the metal oxide layer was kept to be not larger than 1; and the active area of the layer was relatively large, 1.5 cm^2. Table 1B collects the values of the short circuit currents (J_{SC}) and open circuit voltages (V_{OC}) of the devices. A cell made of Al_2O_3 nanoparticles instead of TiO_2 material was used as a reference system for which the internal deactivation of the dyes should be similar to that on TiO_2, but no electron transfer process occurs due to the large bandgap of the Al_2O_3 semiconductor.[26−28] Indeed, a negligible photocurrent for HY103+CDCA/Al_2O_3/AN-50 is observed. For the titania solar cells, the trend in J_{SC} and V_{OC} values is similar to that observed for opaque cells (Table 1A), but, as expected, the photocurrents are lower. J_{SC} in transparent cells is 4−6 times lower than in optimized opaque devices, and V_{OC} is also lower due to lower Fermi level of electrons in titania with a smaller number of photoinduced electrons. Among transparent cells the photocurrent is 5 times higher for EL3 than that for EL2 and AN-50 electrolytes (Table 1B). J_{SC} for EL1 (containing TBP) is lower than that for EL2 (without TBP). The cells with and without coadsorbent give similar photocurrents, but V_{OC} is lower for those without CDCA. All the further spectroscopic data were measured with these complete cells, and therefore the changes in the observed dynamics can be directly related to the differences in the measured photocurrents.

The absorption (maximum intensity at 614 nm) and emission (maximum intensity at 658 nm) spectra of HY103 in DCM solution are shown in Figure S1A (in the Supporting Information). The Stokes shift between absorption and emission band maxima is relatively small (1100 cm^{-1}), and it is not much changed with respect to that in acetonitrile (1400 cm^{-1}),[29] the solvent of much higher polarity. This means that the change in the dipole moment between S_0 and S_1 states of HY103 is not large.

Figure 2A shows the visible absorption spectrum of the selected TiO_2/AN-50 solar cells with and without CDCA (HY103+CDCA/TiO_2/AN-50 and HY103/TiO_2/AN-50 samples), while Figure S1B (Supporting Information) presents the same for TiO_2/EL2 samples. The absorption intensity maximum for the samples with CDCA is at 640 ± 5 nm and should be assigned to the monomer absorbed on metal oxide particles. Interestingly, without coadsorbent an additional blue-shifted band at around 600 nm appears, and it is due to dye aggregates. The classical exciton theory predicts a splitting of the excited state into higher and lower exciton band in the aggregates, so their absorption and fluorescence properties depend on the geometrical distribution of the monomer units in the aggregate.[30] The absorption blue shift is characteristic for H-type of aggregates that form parallel stacking dyes, as expected for molecules absorbed close to each other on the nanoparticle. Moreover, in H-aggregate the transition between the ground to the lower exciton state is forbidden, so they show negligible emission.[30] It can be noted that a shoulder at 600 nm is also present for the samples with CDCA (Figure 2A and Figure S1B, Supporting Information), which means that although the formation of H-aggregates is decreased the aggregates also exist, to some extent, in these samples.

dx.doi.org/10.1021/jp410106k | J. Phys. Chem. C 2014, 118, 194−205

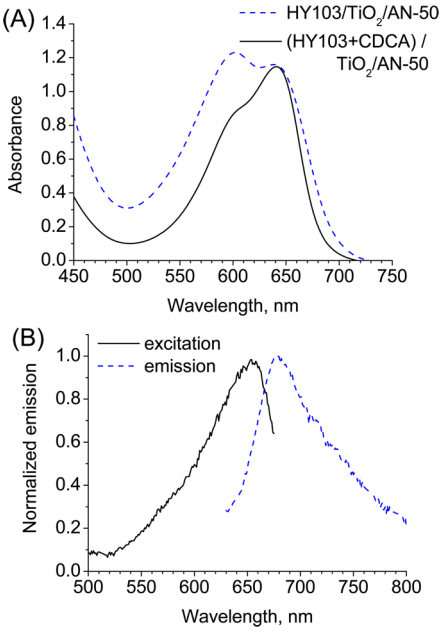

Figure 2. (A) Stationary visible absorption spectra of solar cells made of TiO_2 sensitized with TH305 with or without coadsorbent (CDCA) and filled with AN-50 electrolyte. (B) Stationary emission spectra (excitation at 580 nm) and excitation spectra (emission at 700 nm) of the HY103+CDCA/TiO_2/AN-50 sample.

Transient absorption results presented below will further confirm their presence. The ratio of the absorbance at 600 nm to that around 640 nm (with respect to the corresponding ratio in solution) can give an estimation about the aggregation content. We found that the amount of aggregates is about 10% of that of monomers in all the samples with coadsorbent (HY103+CDCA), while it is about 25% for the HY103/TiO_2/EL2 and about 50% for HY103/TiO_2/AN-50 samples (both without CDCA).

The emission spectrum of solar cells has the maximum around 680 nm (Figure 2B), with a small Stokes shift (about 900 cm^{-1}) with respect to the absorption band. Similar absorption and emission bands were observed for HY103 on Al_2O_3. The lack of any shoulder at 600 nm in the fluorescence excitation band (also presented in Figure 2B) shows that there is no emission from H-aggregates.

The cells with different electrolytes are made with the same TiO_2 nanoparticle film; therefore, the efficiency of charge collection (taking place in the millisecond time scale) is the same for all devices. Thus, to explain the observed differences in photocurrent and global efficiency of the solar cells, time-resolved spectroscopic studies in a shorter time regime are necessary. Flash photolysis experiments on the nanosecond to microsecond time scale were performed to compare dye regeneration quantum yield. To obtain the latter values, a reference cell filled with bulk ACN (instead of electrolytes) was also measured, for which only the process of electron recombination from the semiconductor to the dye radical cation occurs. Figure S2 (Supporting Information) presents the initial transient absorption spectra after excitation at 640 nm. They have a positive maximum between 470 and 480 nm, corresponding to the absorption of the HY103 radical cation (formed after electron injection), and a negative part with maximum around 650 nm due to ground-state depopulation of HY103. The kinetic traces measured close to the positive maximum are shown in Figure 3, while the results of stretched exponential fit are collected in Table 2. The electron

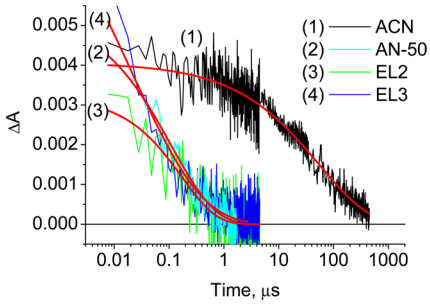

Figure 3. Transient absorption kinetics for HY103+CDCA/TiO_2 cells filled with ACN or indicated electrolytes measured at 480 nm under a pump pulse of 300 $\mu J/cm^2$ at 640 nm. The solid red lines show the best stretched exponential function fit with the parameters given in Table 2.

Table 2. Values of the Parameters of the Best Stretched Exponential Function Given by Equation 1 Fitted to the Transient Absorption Signals Obtained in Flash Photolysis Experiment for the Indicated HY103 Cells[a]

sample	$\tau/\mu s$	β	$k/\mu s^{-1}$	$\phi_{reg}/\%$
TiO_2/ACN	55	0.47	0.008	-
TiO_2/AN-50	0.11	0.56	5.500	99.8
TiO_2/EL2	0.17	0.69	4.600	99.8
TiO_2/EL3	0.02	0.33	8.000	99.9

[a]The excitation and probe wavelengths were 640 and 480 nm, respectively. k is the averaged decay rate constant calculated using eq 2. The regeneration quantum yield, ϕ_{reg}, was calculated using eq 5 and eq 6.

recombination observed for the cell with ACN takes place with the averaged rate constant of 0.008 μs^{-1}. For solar cells with electrolytes, the kinetics of the radical cation decay are about 3 orders of magnitude faster due to the dye regeneration by redox couple, varying the rate constant from 4.6 to 8.0 μs^{-1} for EL2, AN-50, and EL3 electrolytes. This result means that for all electrolytes considered here the quantum yield of dye regeneration is close to 100% (Table 2), and it is not a process influencing the amount of photocurrent for the studied HY103 solar cells. It is not surprising because all electrolytes studied are liquid ones and based on I^-/I_3^- redox couple, so the electrolyte penetration and driving force for electron dye regeneration are similar for all studied configurations. Therefore, the differences in observed solar cell performance have to be connected with electron injection quantum yield, for which studies and discussion in the femtosecond–picosecond time domain are reported in the next sections.

3.3. Femto- to Picosecond Studies of Reference Systems. The femtosecond to picosecond transient absorption measurements were performed in the spectral range of 420–720 nm and the temporal range of 0–500 ps. The pumping pulse was at 580 or 645 nm. For femtosecond upconversion measurement, the pumping pulse was varied from 580 to 665 nm, and the gated emission wavelength was from 680 to 720 nm. Before the results of complete solar cells with titania layer are shown, we will first present the transient femtosecond to picosecond time-resolved studies of reference systems, which is HY103 dye in solution and in the cells with Al_2O_3.

dx.doi.org/10.1021/jp410106k | J. Phys. Chem. C 2014, 118, 194–205

Figure S3A (Supporting Information) presents transient absorption spectra (TAS) for different time delays between the pump and probe for HY103 in DCM solution after excitation at 580 nm. Figure 4A shows wavelength-dependent amplitudes of

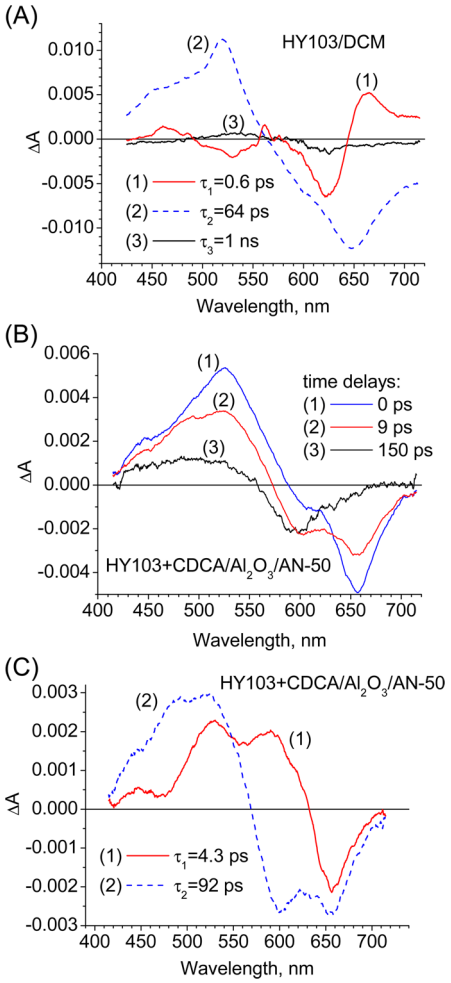

Figure 4. (A) Wavelength-dependent amplitudes of the components having time constants given in the inset and obtained by multiexponential global fit for HY103/DCM under excitation at 580 nm. (B) Transient absorption spectra of HY103+CDCA/Al_2O_3/AN-50 for selected, indicated time delays between the pump (at 645 nm) and probe pulses. (C) The wavelength-dependent amplitudes of the components having time constants given in the inset and obtained by multiexponential global fit for HY103+CDCA/Al_2O_3/AN-50 under excitation at 645 nm.

the time components obtained from multiexponential global analysis of the same TAS. The negative sign of the amplitudes at a given wavelength indicates a rising component (a change toward more positive ΔA value) and a positive sign of the amplitude a decaying component (a change toward more negative ΔA value). The transient absorption signal of HY103 consists of a positive part below 550 nm, originating from the absorption of the S_1 state, and a negative part above 550 nm due to both ground-state depopulation and stimulated emission from S_1. The fastest dynamics of HY103/DCM, taking place with time constant of about 0.6 ps (Figure 4A), is assigned to a solvation process as it exhibits a red shift of the negative stimulated emission band (Figure S3A, Supporting Information). Further evolution due to the decay of the relaxed excited state of HY103 proceeds with a time constant of 64 ps. The transient absorption results are in very good agreement with the fluorescence lifetime obtained in upconversion experiment. The fit to the emission transient measured at 680 nm (in the red part of the fluorescence spectrum, compare with Figure S1A, Supporting Information) is presented in Figure S3B (Supporting Information), and it gives 63 ps as a decay time constant for HY103/DCM. The HY103 fluorescence lifetime was also measured in ACN-based AN-50 electrolyte, for which a much shorter 16 ps time constant is obtained. This latter lifetime value is similar to the reported one for HY103 in ACN solution (~14 ps).[29] This means that the electrolyte compositions in ACN do not influence the HY103 lifetime which depends mainly on the properties of the bulk solvent (shorter in more polar solvent, ACN vs DCM). The short lifetime of HY103 was rationalized by the flip of the C=C bond in the excited state leading to proximity of S_1 and S_0 potential-energy surface at twisted geometry (conical intersection point) and fast S_1–S_0 internal conversion, as confirmed by temperature measurements and theoretical calculations.[29] It is quite likely that the small residual transient absorption signal observed for HY103/DCM (with a 1 ns time constant, see Figure 4A) reflects a conformational photoproduct of such twist in HY103. With all these results in mind, it is reasonable to ask why a dye with such short lifetime gives relatively good efficiencies in DSSCs with ACN-based electrolytes. Our next results will give clues to answer this question.

Figure 4B presents TAS at different time delays between pump and probe for the HY103+CDCA/Al_2O_3/AN-50 sample after excitation at 645 nm, while Figure 4C shows wavelength-dependent amplitudes of the time components obtained from multiexponential global analysis of TAS. It is clear that the dynamics of HY103 adsorbed on the Al_2O_3 surface (without electron injection possibility) is different from that in solution. There is no indication of solvation dynamics, but a fast time constant of 4.3 ps is connected with a recovery of the bleaching band of the HY103 monomers around 650 nm and simultaneous increase of the negative depopulation band at 600 nm, where H-aggregates absorb (see previous section). It can be for example observed in Figure 4B comparing the spectra at 0 and 9 ps delays or in Figure 4C for the amplitude of the 4.3 ps component (negative near 650 nm and positive near 600 nm). This is a clear indication of energy transfer between the monomers and H-aggregates: the population of excited monomers decreases, and that of excited H-aggregates increases. At first sight, such energy transfer is not likely to occur because the classical requirement of the energy transfer mechanism (for example in Förster or Dexter theory) is a good overlap between donor emission and acceptor absorption bands. This condition is certainly not fulfilled for energy transfer to H-aggregates, which have the absorption band blue-shifted with respect to the monomer emission one. It is opposite to J-aggregates, for which absorption is red-shifted and for which the energy transfer from monomers is often considered.[31] As mentioned before, the exciton theory predicts a splitting of the excited state of the monomer into two excited states of aggregates: for J-aggregates the transition to lower exciton level (m_-) is allowed (red shift of absorption band), while the direct excitation to this level (as well as emission from this level) is forbidden for H-aggregates. However, this level can be accessed either after a direct allowed transition to the higher exciton state of H-aggregates (m_+, causing blue shift of absorption band) or after the energy transfer from the excited

dx.doi.org/10.1021/jp410106k | J. Phys. Chem. C 2014, 118, 194–205

state of the monomer, which lies higher. This situation is shown in Scheme 1 with the rate constant, k_{ET}, of energy transfer from

Scheme 1. Scheme of Deactivation of HY103 Dyes in DSSCs: Red and Blue Solid Arrows Indicate the Excitation of Monomers and H-Aggregates, Respectively, While the Dotted Red Line Indicates an Emission from Monomers (Radiative Rate k^M_R)[a]

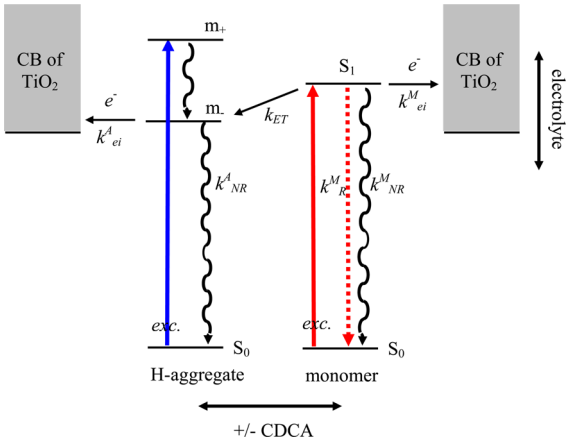

[a]The nonradiative deactivation in both monomers (rate k^M_{NR}) and H-aggregates (rate k^A_{NR}) is indicated by waved arrows, and solid arrows show the electron and energy transfer processes: electron injection from monomer to TiO_2 (rate k^M_{ei}), electron injection from H-aggregate to TiO_2 (rate k^A_{ei}), and energy transfer from the S_1 state of the monomer to the energy transfer process to the lower level of the H-aggregate exciton band (m_). The electrolyte composition can change the relative position of the conduction band edge in TiO_2, and adding coadsorbent (CDCA) influences the aggregation degree of HY103 dyes on nanoparticles.

the S_1 state of monomers to the m_ state of H-aggregates. Therefore, more precise examination of the nature of energy levels in aggregates confirms the possibility of quenching the monomers by H-aggregates, and in fact such a process was previously reported.[32,33] However, according to our knowledge, this process has not been considered so far in the studies of DSSCs. In DSSC interfacial systems the formation of H-aggregates is favored over J-aggregates.[34] Thus, our direct finding of the energy transfer from monomers to H-aggregates is novel and could explain the photobehavior of other dyes used in the DSSC field.

Another, longer time constant from the global fit for the HY103+CDCA/Al_2O_3/AN-50 sample (92 ps, Table 3) originates from the decay of lower exciton state of H-aggregates (with rate constant, k^A_{NR}, Scheme 1). However, Figure 4C shows the spectral changes taking place with this time constant involve not only the recovery of the ground state of the aggregates (at 600 nm) but also that of monomers (at 650 nm). This means that the value of longer time constant might by affected by the slower part of the energy transfer process from monomers to aggregates. Indeed, when a 3-exponential global fit model is used instead of a 2-exponential one (Figure S4, Supporting Information), the slower part of the ground-state recovery of monomers (52 ps, due to energy transfer) is found to occur faster than the slower part of the ground-state recovery of aggregates (177 ps, due to their nonradiative decay). Another confirmation of nonsingle exponential kinetics for energy transfer comes from the time-dependent fluorescence studies (Figure 5A and Table 4A). In the fluorescence

Table 3. Summary of Femtosecond to Picosecond Transient Absorption Studies[a]

cell	τ_1, ps	τ_2, ps	k^A_{ei}/ps^{-1}	ϕ^A_{ei}/%	r
HY103+CDCA/Al_2O_3/AN-50	4.3	92	-	-	0
HY103+CDCA/TiO_2/EL2	3.3	45	0.011	50	0.12
HY103+CDCA/TiO_2/AN-50	3.6	47	0.010	48	0.17
HY103+CDCA/TiO_2/EL3	1.5	13	0.066	86	0.52

[a]Shorter (τ_1) and longer (τ_2) time constants were obtained from global multiexponential fit. Electron injection rate constant from monomers, k^A_{ei}, was obtained from eq 3 based on τ_2 values. The electron injection quantum yield, ϕ^A_{ei}, was calculated from eq 4. The last column shows the ratio of the residual transient absorption signal at the maximum of radical cation band to the initial transient absorption signal at the maximum: $r = \Delta A(475\text{ nm}, 500\text{ ps})/\Delta A(515\text{ nm}, 0\text{ ps})$.

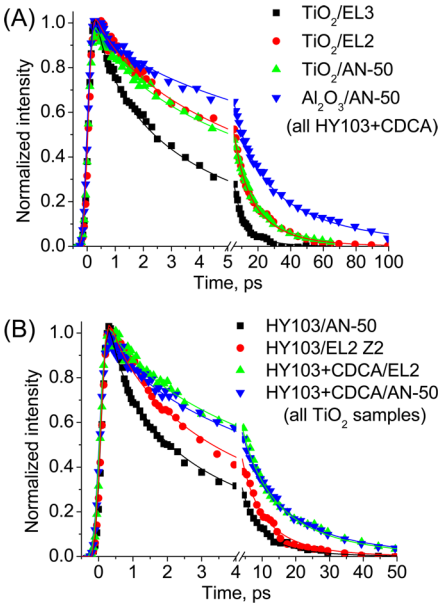

Figure 5. Femtosecond emission transients of (A) HY103+CDCA samples with TiO_2 or Al_2O_3 and different electrolytes and (B) solar cells with electrolytes EL2 or AN-50 sensitized with HY103 with or without CDCA. The emission was observed at 680 nm and upon excitation with 500 nJ/cm^2 pulses at 620 nm. The solid lines are from the best fit using the convolution of IRF of the setup with stretched exponential function given by eq 1 and the parameters given in Tables 3A and 3B.

experiment, only monomers are observed (H-aggregates are not fluorescent: its radiative rate constant is small due to the forbidden nature of the transition), and their emission transients cannot be fitted with a single-exponential function. Instead of that, we have used a stretched exponential fit model (Figure 5A) giving an average rate constant of 0.032 ps^{-1} for energy transfer from monomers for aggregates (Table 4A). The reciprocal of this value (31 ps) is longer than the shorter 4.6 ps component obtained from transient absorption.

Therefore, time constants from 2-exponential global fit to transient absorption data are only approximately related to certain processes: the first component (4.3 ps for HY103+-CDCA/Al_2O_3/AN-50 sample) is the fastest part of energy transfer from monomers to aggregates, while the second component (92 ps) is mainly due to decay of aggregates; however, it is also affected by the slower part of energy transfer. However, using more components in multiexponential global fit

dx.doi.org/10.1021/jp410106k | J. Phys. Chem. C 2014, 118, 194−205

Table 4. Values of the Parameters of HY103 Cells Obtained from Time-Resolved Fluorescence Studies[a]

(A)

sample	τ/ps	β	k/ps^{-1}	k^{M}_{ei}/ps^{-1}	ϕ^{M}_{ei}/%
HY103+CDCA/Al_2O_3/ AN-50	15.7	0.59	0.041	-	-
HY103+CDCA/TiO_2/AN-50	7.3	0.62	0.095	0.054	57
HY103+CDCA/TiO_2/EL2	7.3	0.65	0.100	0.059	59
HY103+CDCA/TiO_2/EL3	2.5	0.58	0.254	0.213	84

(B)

sample	τ/ps	β	k/ps^{-1}
HY103/TiO_2/AN-50	2.0	0.56	0.302
HY103/TiO_2/EL2	3.8	0.64	0.189

[a] τ and β are the parameters of stretched exponential function given by eq 1 convoluted with IRF (FWHM = 300 fs) fitted to the emission transient at 680 nm with the excitation laser pulses at 620 nm. k is the averaged decay rate constant calculated using eq 2. (A) Parameters for cell made of HY103 and CDCA and filled with different electrolytes. Electron injection rate constant from monomers, k^{M}_{ei}, was obtained using eq 3. The electron injection quantum yield, ϕ^{M}_{ei}, was calculated using eq 4. (B) Parameters of solar cells made of HY103 without coadsorbent and filled with two electrolytes.

in the solar cells with titania (where additional radical cation species are present, see next section) resulted in strong correlations of the time constants and spectra due to the limited signal-to-noise ratio and the nonexponential nature of both energy and electron transfer processes. Thus, only a 2-exponential model for the processes in monomers and aggregates will be used to estimate the electron injection contribution in the transient absorption results presented in the next section.

3.4. Femto- to Picosecond Studies of Transparent Solar Cell. Figure 6A shows the TAS of the solar cell of the best efficiency, HY103+CDCA/TiO_2/EL3, and Figure 6B exhibits the results of a global analysis leading to wavelength-dependent amplitudes of the fitted time components. Compared to the reference (Al_2O_3 system), an additional component of a long lifetime (τ_3 =1 ns, acting as a constant background in the 500 ps time window of the experiment) is necessary to obtain a good quality of the fit. The spectrum of this component is assigned to the HY103 radical cation, obviously not present in the results using the Al_2O_3 system. Its spectral shape is similar to that observed in flash photolysis studies (Figure S2, Supporting Information). Moreover, the spectra of the two faster components (τ_1 = 1.5 ps and τ_2 = 13 ps, Figure 6B) are similar to those for the Al_2O_3 cell (Figure 4C), but the time constants are significantly shorter. This means that both energy transfer from monomers to aggregates and the decay of aggregates are affected by efficient electron injection. The electron injection taking place from monomers to TiO_2 (with the rate k^{M}_{ei}) competes with energy transfer and decreases the value of the first time constant, while the electron injection from H-aggregates to TiO_2 (with the rate k^{A}_{ei}) accelerates the overall decay of these species, so decreases the value of the second time constant (Scheme 1).

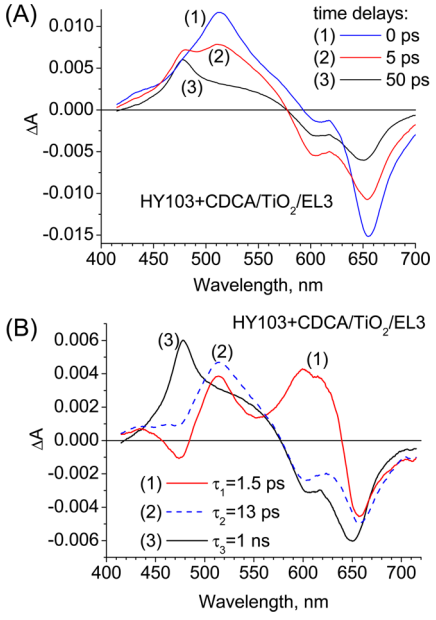

Figure 6. (A) Transient absorption spectra of HY103+CDCA/TiO_2/EL3 for selected, indicated time delays between the pump (at 645 nm) and probe pulses. (B) The wavelength-dependent amplitudes of the components having time constants given in the inset and obtained by multiexponential global fit for HY103+CDCA/TiO_2/EL3 under excitation at 645 nm.

Figures 7A and 7B show the analogous global analysis results of transient absorption studies for solar cells of other electrolytes with lower performance: HY103+CDCA/TiO_2/AN-50 and HY103+CDCA/TiO_2/EL2, respectively. Figures S5A and S5B (Supporting Information) show their original TAS at different pump−probe time delays. Here, the radical cation contribution (the third component) is significantly smaller than for HY103+CDCA/TiO_2/EL3. The first and second time constant (3.3−3.6 ps and 45−47 ps) are shortened compared to the Al_2O_3 system but not so much as for EL3 electrolyte. This clearly indicates that electron injection is slower for AN-50 and EL2. Table 3 gives the values of transient absorption time constants from global analysis for solar cells with the three electrolytes and Al_2O_3 reference system. The longer component observed for Al_2O_3 (τ_2 = 92 ps) serves as a measure of nonradiative decay of excited H-aggregates on the nanoparticles ($k^{A}_{NR} = 1/\tau_2$ = 0.011 ps^{-1}). The obtained values permit calculation of electron injection rate from aggregates and the quantum yield of this process (ϕ^{A}_{ei}). As can be seen, the electron injection is about 6 times faster for EL3 (with only Li^+ in electrolyte, k^{A}_{ei} = 0.066 ps^{-1}) than for EL2 (k^{A}_{ei} = 0.011 ps^{-1}) and AN-50 (k^{A}_{ei} = 0.010 ps^{-1}). Interestingly, the electron injection rates for AN-50 electrolyte (based on Li cations but also containing TBP) are similar to that for EL2 (without TBP but with a similar amount of guanidine cation instead of Li^+). It also agrees with the same photocurrent observed for both these cells (Table 2). This again indicates that the shift of the TiO_2 conduction band edge toward more positive potential is much

dx.doi.org/10.1021/jp410106k | J. Phys. Chem. C 2014, 118, 194−205

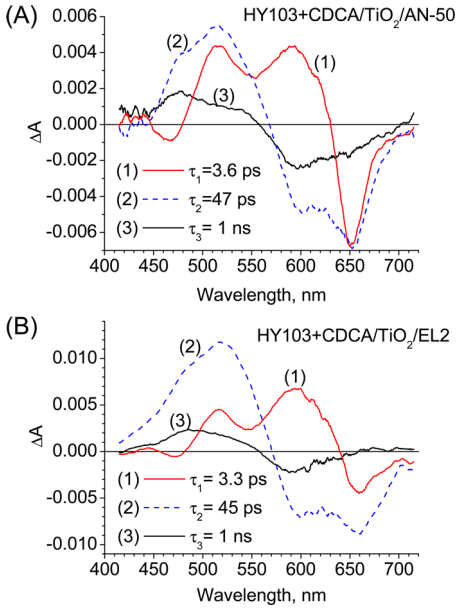

Figure 7. Wavelength-dependent amplitudes of the components having time constants given in the inset and obtained by multi-exponential global fit for (A) HY103+CDCA/TiO_2/AN-50 and (B) HY103+CDCA/TiO_2/EL2, all under excitation at 645 nm.

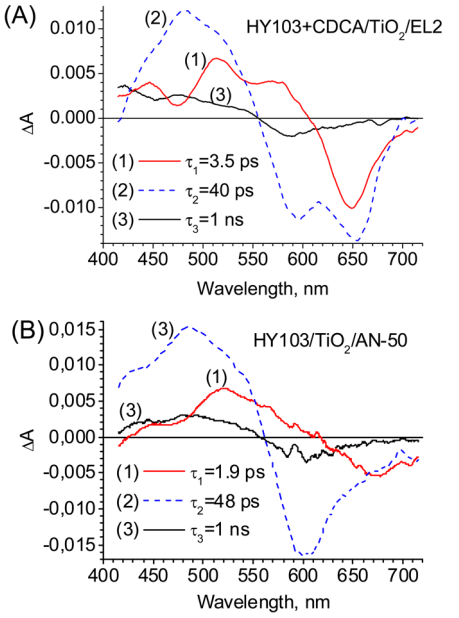

Figure 8. Wavelength-dependent amplitudes of the components having time constants given in the inset and obtained by multi-exponential global fit of the signals from (A) HY103+CDCA/TiO_2/EL2 and (B) HY103/TiO_2/AN-50, both under excitation at 580 nm.

higher for much smaller Li cations, because the opposite effect of TBP brings it to the same potential as for larger guanidine cations without TBP.

The last column of Table 3 presents the ratio (r) of the amplitude at the maximum of radical cation spectra for long time delays (at 475 nm and t = 500 ps, sufficiently long that no excited monomers or aggregates will be present) to the initial amplitude of the maximum of transient absorption signal (at 515 nm and t = 0 ps). Therefore, the value of r is proportional to the final population of the radical cation and thus reflects the amount of injected electron in the TiO_2 conduction band after an initial charge separation process. The values of r are 3−4 times larger for EL3 than for AN-50 and EL2 (Table 3), a behavior in a good agreement with that of the ratio of the photocurrents in these solar cells (Table 1B). Thus, the global parameter of the solar cell (J_{SC}) is nicely correlated with the observation in ultrafast time-resolved studies.

All the results presented in Figures 6 and 7 and collected in Table 3 were obtained for the excitation at 645 nm, where there is a maximum of monomer absorption. To further support the proposed deactivation mechanism of HY103 in DSSCs, experiments with excitation at 580 nm were performed. At this wavelength, relatively more aggregates (absorption maximum at 600 nm) are directly excited. Figure 8A presents the global analysis for HY103+CDCA/TiO_2/EL2 (and Figure S6A, Supporting Information, shows the spectra for different time delays). The sample is the same one used to get the result shown in Figure 7B (and Figure S5B, Supporting Information). By comparing the corresponding figures (for example, the spectra of the τ_1 component in Figure 8A and Figure 7B), we can observe initially more aggregates, and the relative increase of additional population of aggregates formed from excited monomers is smaller for excitation at 580 than at 645 nm. However, the time constants are similar. Much more drastic changes are observed for the HY103/TiO_2/AN-50 solar cell excited at 580 nm (Figure 8B and Figure S6B, Supporting Information). In this case the contribution of aggregates is enhanced not only because of the excitation wavelength but also because of their higher concentration (due to the lack of coadsorbent). Indeed, the bleaching of the monomer band and its evolution due to energy transfer has much smaller amplitude for this sample than for those shown before. It is also remarkable that the shortest time constant (1.9 ps, Figure 8B) is almost 2 times shorter than that for the sample with CDCA and the same electrolyte (3.6 ps, Figure 7A), while the second time constant is similar in both cases. This indicates that the decay rates of aggregates are similar in magnitude, but the energy transfer from monomers to H-aggregates becomes faster when the concentration of aggregates increases. This is further investigated below in time-resolved fluorescence studies.

The time-resolved fluorescence studies only probe monomers' transients so they permit more precise calculation of electron injection rate constant from these species to the titania conduction band. Figure 5A shows the emission transients of HY103+CDCA solar cells (and the reference sample with Al_2O_3) observed at 680 nm (maximum of the emission band) with the fits using stretched exponential functions. The parameters of the fits are collected in Table 4A, together with the calculated electron injection rate constants from monomers and the quantum yields of this process. The fastest electron injection takes place for EL3 (k^M_{ei} = 0.213 ps^{-1}), while for electrolytes AN-50 and EL2 it is about 4 times slower (k^M_{ei} = 0.054 ps^{-1} and k^M_{ei} = 0.059 ps^{-1}, respectively). Therefore, the same trend is observed as for the electron injection from aggregates (discussed above), but in the case of monomers the rate constants are 3−5 times faster. This is quite understandable because the S_1 state of monomers lies higher than the m_- state of aggregates. Assuming that the S_1 state is in the middle between m_+ and m_- states (Scheme 1) and based on the absorption maxima of monomers and aggregates, the difference of the electron injection level is about 1150 cm^{-1} which corresponds to the potential change of 140 mV.

When a more relaxed state of monomers is probed (emission at 700 nm instead of 680 nm) then both the rates of energy

dx.doi.org/10.1021/jp410106k | J. Phys. Chem. C 2014, 118, 194−205

transfer and electron injection are slightly smaller (by about 20%). These results are presented in Figures S7 and S8 (Supporting Information). Figure S9A (Supporting Information) shows that the observed emission transients do not depend on the excitation wavelength, while Figure S9B (Supporting Information) confirms that they are also independent of the excitation pulse fluence. The latter results means that no singlet−singlet annihilation process occurs that frequently disturbs the ultrafast observation in DSSC systems.[34]

Finally, Figure 5B shows a comparison between solar cells with and without coadsorbent for AN-50 and EL2 electrolytes. The higher the concentration of H-aggregates, the faster is the decay of fluorescence transients due to the increase in the energy transfer rate constant from monomers to aggregates. The parameters of the stretched exponential fit and the average rates of the fluorescence decay (k) are summarized in Table 4B. Assuming that electron injection rate from monomer (k^{M}_{ei}) is the same for different concentrations of aggregates, it is possible to calculate the sum of the rest of the deactivation rates ($k^{M}_{R} + k^{M}_{NR} + k^{M}_{ET} = k - k^{M}_{ei}$, see Scheme 1). These rate constants are 0.25 ps^{-1} for HY103/TiO_2/AN-50, 0.14 ps^{-1} for HY103/TiO_2/EL2, and about 0.04 ps^{-1} for both HY103+CDCA/TiO_2/AN-50 and HY103+CDCA/TiO_2/EL2. These values linearly correlate with the previously estimated relative concentrations of H-aggregates (50% for HY103/TiO_2/AN-50, 25% for HY103/TiO_2/EL2, and 10% for HY103+CDCA/TiO_2/AN-50 and HY103+CDCA/TiO_2/EL2, see above). This indicates that the values of k^{M}_{ET} dominate in the rest of the deactivation rates (apart from k^{M}_{ei}) and that internal conversion in monomers does not play a significant role in the deactivation of its S_1 state ($k^{M}_{R} + k^{M}_{NR} < 0.01$ ps^{-1}). Interestingly, the internal conversion rate constant for H-aggregates (calculated above) is also small, $k^{A}_{NR} = 0.01$ ps^{-1}.

In principle, we cannot exclude that components having times shorter than our time resolution are missed in our analysis. It could be possible that there is an additional ultrafast electron injection process from monomers to the titania conduction band of time constant <100 fs. Such a process should be accompanied in TAS by a decrease of stimulated emission (SE) band intensity, while ground-state depopulation intensity is not changed. To examine this possibility, we separated ground-state depopulation and SE signals by subtracting the stationary absorption and fluorescence spectra from initial TAS (Figure S10, Supporting Information). Although the subtraction procedure is a little bit arbitrary, it is clear from Figure S10 (Supporting Information) that the relative contribution of SE (above 620 nm) intensity in the full signal is similar for the HY103/DCM system (Figure S10A, Supporting Information), the reference Al_2O_3 sample (without electron injection, Figure S10B, Supporting Information) and the TiO_2 one (with electron injection, Figure S10C, Supporting Information). This means that there are rather not any electron injection processes from HY103 occurring faster than IRF (150−200 fs) of our setups.

Having presented and discussed the above results, we now go back to the issue raised in section 3.2 concerning quick decay of free HY103 in ACN and ACN-based electrolyte (16 ps). The lifetime of both monomers and H-aggregates attached to the nanoparticles is about 100 ps or more when electron injection and energy transfer are not considered. Most probably, this is because the rotation around the C═C bond in the excited state (that leads to the fast deactivation in solution) is slowed down in restricted conditions when molecules are packed close to each other on the nanoparticle surface. Therefore, the prolongation of the lifetime is enough to permit high quantum yield of electron injection. It is in contrast with our previous studies of dyes for DSSCs in which a shortening of the lifetime of the dye on Al_2O_3 with respect to that in solution was observed.[35] This new finding on systems when the situation is reversed should be quite important in designing dyes for DSSCs and for predicting their efficiencies.

4. CONCLUSIONS

We presented combined global efficiency and spectroscopic studies of a DSSC made of HY103, recently introduced near IR absorbing dye for the applications in tandem cells. The effect of coadsorbent (CDCA), size of cations in electrolyte (Li vs guanidine), and addition of TBP is investigated. The current−voltage characteristic of the opaque solar cells reveals that only for the electrolyte with LiI (0.06 M) and without TBP the system shows good enough global efficiency (η = 2.7%). When higher concentration of LiI is used (0.5 M), the solar cell performance decreases (η = 2.4%), although a higher photocurrent is reached. When guanidine thiocyanate is used (instead of LiI) or TBP is added, the efficiency of the cell drastically decreases (η < 1%). The solar cell efficiency improves when coadsorbent is added for sensitization.

The stationary visible absorption spectroscopic studies show the presence of monomers with an absorption band at 650 nm and H-aggregates with an absorption at 600 nm. Their relative concentration depends on the presence of coadsorbent (CDCA). Macroscopic parameters (J_{SC} and V_{OC}) of the different cells are well correlated with the results of time-resolved transient absorption and emission studies made for transparent cells. First, nanosecond flash photolysis studies show that the dye regeneration rate constant (k_{reg} = 4.6−8.0 μs^{-1}) is much faster than the electron recombination one (k_{recom} = 0.008 μs^{-1}); therefore, regeneration quantum yield is close to 100% for all studied iodide-based electrolytes. The differences in photocurrents are thus due to the ultrafast processes, as revealed in combined femtosecond to picosecond transient absorption and upconversion studies. Second, the electron injection rate constant from HY103 monomers is k^{M}_{ei} = 0.21 ps^{-1} for electrolyte with only Li^+ (EL3) and drops down to k^{M}_{ei} = 0.05 ps^{-1} when either TBP is added (AN-50) or guanidine cations are used instead of Li^+ (EL2). Third, the electron injection rate constant from H-aggregates (k^{A}_{ei} = 0.07 ps^{-1} for EL3 and k^{A}_{ei} = 0.01 ps^{-1} for EL2 or AN-50 electrolytes) is smaller than that from monomers. The results are explained by the effect of changing the potential of TiO_2 conduction band edge with different composition of iodide-based electrolyte that affects electron injection quantum yield. For HY103 with the redox potential of the excited state much more positive than that of many dyes for DSSCs, it is necessary to add small cations (Li^+) without pyridine base to lower the energetic position of the conduction band and facilitate efficient electron injection.

Finally, two important findings are revealed which are quite novel in DSSC studies. First, fast energy transfer from the S_1 state of the monomer to a lower exciton band of H-aggregate (m_) is found. The rate constant of this process depends on the relative concentration of H-aggregates: k_{ET} = 0.04 ps^{-1} for 10%, k_{ET} = 0.14 ps^{-1} for 25%, and k_{ET} = 0.25 ps^{-1} for 50% of aggregates concentration. We also found that the rate constant of nonradiative decay of the excited state of HY103 on nanoparticles ($k^{M}_{NR} < 0.01$ ps^{-1} for monomers and k^{A}_{NR} = 0.01

dx.doi.org/10.1021/jp410106k | J. Phys. Chem. C 2014, 118, 194−205

ps^{-1} for H-aggregates) is several times slower than that of HY103 in solution (lifetime of 16 ps in ACN). This is explained by the restriction of the twisting of the HY103 molecule around the C=C bond (that governs the dye deactivation in solution) when the dye molecules are attached to the nanoparticle. The overall deactivation scheme of complete DSSCs made of HY103 is shown in Scheme 1.

It should be emphasized that our findings are not only limited to infrared dyes but also of general importance in the DSSC field, also for dyes absorbing in the visible range. Adding a coadsorbent to prevent dye aggregation is a commonly used procedure for different groups of dyes, including porphyrins and all-organic ones. We showed that the aggregation can be formed, to some extent, even when the coadsorbent is used, and we believe that the mechanism of energy transfer between monomers and aggregates, revealed in this work, can operate in many other DSSC systems. Flexible double bonds are a frequent feature of many organic dyes for solar cells and are responsible for their short lifetimes in solution compared to ruthenium or porphyrin compounds. Our results show that in such dyes, after attachment to the nanoparticles, the electron injection quantum yield can still be very high. Finally, the ultrafast time-resolved studies of initial charge separation processes in complete DSSCs are still not well documented, so our findings of the electron injection rate dependence on electrolyte composition should significantly contribute to such universal knowledge.

■ ASSOCIATED CONTENT

Supporting Information

Figures S1−S10 and Tables S1−S2 (stationary absorption and emission of HY103/DCM, ns transient absorption spectra of HY103 cells, fs transient absorption spectra and emission transients of HY103/DCM, transient absorption spectra and emission transients of HY103 cells, emission parameters obtained from the fits and the effect of stationary absorption and fluorescence subtraction from the fs transient absorption). This material is available free of charge via the Internet at http://pubs.acs.org.

■ AUTHOR INFORMATION

Corresponding Authors

*E-mail: marziol@amu.edu.pl. Tel.: +48 61 829 5011 (M.Z.).
*E-mail: abderrazzak.douhal@uclm.es. Tel.: +34 925 265717 (A.D.).

Notes

The authors declare no competing financial interest.

■ ACKNOWLEDGMENTS

This work was supported by NCN (National Science Centre in Poland) project 2012/05/B/ST3/03284 and MINECO (Spain) through projects PLE2009-0015 and MAT2011-25472. Femtosecond transient absorption studies were made at the Center for Ultrafast Laser Spectroscopy at the A. Mickiewicz University in Poznan, Poland. Femtosecond upconversion and flash photolysis experiments were done at the UCLM (Toledo, Spain). We thank professor Xichuan Yang (DUT) and professor Licheng Sun (DUT and KTH) for the support of this project and valuable discussions. M.Z. thanks the UCLM for the financial support for his stay.

■ REFERENCES

(1) O'Regan, B.; Grätzel, M. A Low-Cost, High-Efficiency Solar Cell Based on Dye-Sensitized Colloidal TiO2 Films. *Nature* **1991**, *353*, 737−740.

(2) Hagfeldt, A.; Boschloo, G.; Sun, L.; Kloo, L.; Pettersson, H. Dye-Sensitized Solar Cells. *Chem. Rev.* **2010**, *110*, 6595−6663.

(3) Grätzel, M.; Durrant, J. R. Dye-Sensitised Mesoscopic Solar Cells. In *Nanostructured and Photoelectrochemical Systems for Solar Photon Conversion*; Archer, M. D., Nozik, A. J., Eds.; Imperial College Press: London, 2008; pp 503−536.

(4) Yu, Q.; Wang, Y.; Yi, Z.; Zu, N.; Zhang, J.; Zhang, M.; Wang, P. High-Efficiency Dye-Sensitized Solar Cells: The Influence of Lithium Ions on Exciton Dissociation, Charge Recombination, and Surface States. *ACS Nano* **2010**, *4*, 6032−6038.

(5) Yella, A.; Lee, H.-W.; Tsao, H. N.; Yi, C.; Chandiran, A. K.; Nazeeruddin, M. K.; Diau, E. W.-G.; Yeh, C.-Y.; Zakeeruddin, S. M.; Grätzel, M. Porphyrin-Sensitized Solar Cells with Cobalt (II/III)−Based Redox Electrolyte Exceed 12% Efficiency. *Science* **2011**, *334*, 629−634.

(6) Hardin, B. E.; Snaith, H. J.; McGehee, M. D. The Renaissance of Dye-Sensitized Solar Cells. *Nat. Photonics* **2012**, *6*, 162−169.

(7) Moser, J. E. Dynamics of Interfacial and Surface Electron Transfer Processes. In *Dye-sensitized solar cells*; 2010 ed.; Kalyanasundaram, K., Ed.; EPFL Press: Lausanne, 2010; pp 403−456.

(8) Anderson, A. Y.; Barnes, P. R. F.; Durrant, J. R.; O'Regan, B. C. Quantifying Regeneration in Dye-Sensitized Solar Cells. *J. Phys. Chem. C* **2011**, *115*, 2439−2447.

(9) Anderson, A. Y.; Barnes, P. R. F.; Durrant, J. R.; O'Regan, B. C. Simultaneous Transient Absorption and Transient Electrical Measurements on Operating Dye-Sensitized Solar Cells: Elucidating the Intermediates in Iodide Oxidation. *J. Phys. Chem. C* **2010**, *114*, 1953−1958.

(10) Giannouli, M.; Fakis, M. Interfacial Electron Transfer Dynamics and Photovoltaic Performance of TiO2 and ZnO Solar Cells Sensitized with Coumarin 343. *J. Photochem. Photobiol. A: Chem* **2011**, *226*, 42−50.

(11) Koops, S. E.; Durrant, J. R. Transient Emission Studies of Electron Injection in Dye Sensitised Solar Cells. *Inorg. Chim. Acta* **2008**, *361*, 663−670.

(12) Juozapavicius, M.; Kaucikas, M.; van Thor, J. J.; O'Regan, B. C. Observation of Multiexponential Pico- to Subnanosecond Electron Injection in Optimized Dye-Sensitized Solar Cells with Visible-Pump Mid-Infrared-Probe Transient Absorption Spectroscopy. *J. Phys. Chem. C* **2013**, *117*, 116−123.

(13) Haque, S. A.; Palomares, E.; Cho, B. M.; Green, A. N. M.; Hirata, N.; Klug, D. R.; Durrant, J. R. Charge Separation versus Recombination in Dye-Sensitized Nanocrystalline Solar Cells: the Minimization of Kinetic Redundancy. *J. Am. Chem. Soc.* **2005**, *127*, 3456−3462.

(14) Conibeer, G. Third-Generation Photovoltaics. *Mater. Today* **2007**, *10*, 42−50.

(15) Li, L.; Hao, Y.; Yang, X.; Zhao, J.; Tian, H.; Teng, C.; Hagfeldt, A.; Sun, L. A Double-Band Tandem Organic Dye-sensitized Solar Cell with an Efficiency of 11.5%. *ChemSusChem* **2011**, *4*, 609−612.

(16) Tian, H.; Yang, X.; Cong, J.; Chen, R.; Liu, J.; Hao, Y.; Hagfeldt, A.; Sun, L. Tuning of Phenoxazine Chromophores for Efficient Organic Dye-Sensitized Solar Cells. *Chem. Commun.* **2009**, 6288−6290.

(17) Ziółek, M.; Martín, C.; Sun, L.; Douhal, A. Effect of Electrolyte Composition on Electron Injection and Dye Regeneration Dynamics in Complete Organic Dye Sensitized Solar Cells Probed by Time-Resolved Laser Spectroscopy. *J. Phys. Chem. C* **2012**, *116*, 26227−26238.

(18) Hao, Y.; Yang, X.; Cong, J.; Tian, H.; Hagfeldt, A.; Sun, L. Efficient near Infrared D−p−A Sensitizers with Lateral Anchoring Group for Dye-Sensitized Solar Cells. *Chem. Commun.* **2009**, 4031−4033.

(19) Grätzel, M. Conversion of Sunlight to Electric Power by Nanocrystalline Dye-Sensitized Solar Cells. *J. Photochem. Photobiol. A: Chem.* **2004**, *164*, 3−14.
(20) Lee, K. M.; Suryanarayanan, V.; Ho, K. C.; Thomas, K. R. J.; Jiann T. Lin, J. T. Effects of Co-Adsorbate and Additive on the Performance of Dye-Sensitized Solar Cells: A Photophysical Study. *Sol. Energy Mater. Sol. Cells* **2007**, *91*, 1426−1431.
(21) Krasovec, U. O.; Berginc, M.; Hocevar, M.; Topic, M. Unique TiO2 Paste for High Efficiency Dye-Sensitized Solar Cells. *Sol. Energy Mater. Sol. Cells* **2009**, *93*, 379−381.
(22) Maciejewski, A.; Naskręcki, R.; Lorenc, M.; Ziółek, M.; Karolczak, J.; Kubicki, J.; Matysiak, M.; Szymański, M. Transient Absorption Experimental Set-Up with Femtosecond Time Resolution. Femto- and Picosecond Study of DCM Molecule in Cyclohexane and Methanol Solution. *J. Mol. Struct.* **2000**, *555*, 1−13.
(23) Katilius, E.; Hindorff, J.; Woodbury, N. ASUFIT program available at www.public.asu.edu/~laserweb/asufit/asufit.html.
(24) Ardo, S.; Meyer, G. J. Photodriven Heterogeneous Charge Transfer with Transition-Metal Compounds Anchored to TiO2 Semiconductor Surfaces. *Chem. Soc. Rev.* **2009**, *38*, 115−164.
(25) Boschloo, G.; Häggman, L.; Hagfeldt, A. Quantification of the Effect of 4-tert-Butylpyridine Addition to I-/I3 - Redox Electrolytes in Dye-Sensitized Nanostructured TiO2 Solar Cells. *J. Phys. Chem. B* **2006**, *110*, 13144−13150.
(26) Vinodgopal, K.; Hua, X.; Dahlgren, R. L.; Lappin, A. G.; Patterson, L. K.; Kamat, P. V. Photochemistry of Ru(bpy)2(dcbpy)2+ on Al203 and Ti02 Surfaces. An Insight into the Mechanism of Photosensitization. *J. Phys. Chem.* **1995**, *99*, 10883−10889.
(27) Luo, L.; Lo, C.-F.; Lin, C.-Y.; Chang, I.-J.; Diau, E. W.-G. Effects of Aggregation and Electron Injection on Photovoltaic Performance of Porphyrin-Based Solar Cells with oligo(phenylethynyl) Links inside TiO2 and Al2O3 Nanotube Arrays. *Phys. Chem. Chem. Phys.* **2010**, *12*, 1064−1071.
(28) Palomares, E.; Clifford, J. N.; Haque, S. A.; Lutz, T.; Durrant, J. R. Control of Charge Recombination Dynamics in Dye Sensitized Solar Cells by the Use of Conformally Deposited Metal Oxide Blocking Layers. *J. Am. Chem. Soc.* **2002**, *125*, 475−482.
(29) Sun, Q.; Liu, J.; Hao, Y.; Yang, X. Volume-conserved Twist Excited-State of pi-Conjugated Molecules. *Chin. J. Chem. Phys.* **2010**, *23*, 637−642.
(30) Martínez, V. M.; Arbeloa, F. L.; Prieto, J. B.; Arbeloa, I. L. Characterization of Rhodamine 6G Aggregates Intercalated in Solid Thin Films of Laponite Clay. 2 Fluorescence Spectroscopy. *J. Phys. Chem. B* **2005**, *109*, 7443−7450.
(31) de Miguel, G.; Ziółek, M.; Zitnan, M.; Organero, J. A.; Pandey, S. S.; Hayase, S.; Douhal, A. Photophysics of H- and J-Aggregates of Indole-Based Squaraines in Solid State. *J. Phys. Chem. C* **2012**, *116*, 9379−9389.
(32) Wang, Y.; Chen, H.; Wu, H.; Li, X.; Weng, Y. Fluorescence Quenching in a Perylenetetracarboxylic Diimide Trimer. *J. Am. Chem. Soc.* **2009**, *131*, 30−31.
(33) Stevens, N. Nonlinear Optical Switching Properties Of Dye-Doped Inorganic/Organic Composite Films. *PhD thesis*, The City University of New York, 2006.
(34) de Miguel, G.; Marchena, M.; Ziółek, M.; Pandey, S. S.; Hayase, S.; Douhal, A. Femto- to Millisecond Photophysical Characterization of Indole-Based Squaraines Adsorbed on TiO2 Nanoparticle Thin Films. *J. Phys. Chem. C* **2012**, *116*, 12137−12148.
(35) Martín, C.; Ziółek, M.; Marchena, M.; Douhal, A. Interfacial Electron Transfer Dynamics in a Solar Cell Organic Dye Anchored to Semiconductor Particle and Aluminum-Doped Mesoporous Materials. *J. Phys. Chem. C* **2011**, *115*, 23183−23191.